Rare tetranuclear mixed-valent $[Mn^{II}_2Mn^{IV}_2]$ clusters as building blocks for extended networks†‡

Georgios Karotsis,[a] Leigh F. Jones,[a] Giannis S. Papaefstathiou,[b] Anna Collins,[a] Simon Parsons,[a] Tuyen D. Nguyen,[c] Marco Evangelisti[c] and Euan K. Brechin*[a]

Received 25th March 2008, Accepted 23rd June 2008
First published as an Advance Article on the web 1st August 2008
DOI: 10.1039/b804897e

We report the synthesis of a series of mixed valence $Mn^{II/IV}$ tetranuclear clusters $[Mn^{II}_2Mn^{IV}_2O_2(heed)_2(EtOH)_6Br_2]Br_2$ (**1**), $[Mn^{II}_2Mn^{IV}_2O_2(heed)_2(H_2O)_2Cl_4]\cdot2EtOH\cdot H_2O$ (**2**·2EtOH·H_2O), $[Mn^{II}_2Mn^{IV}_2O_2(heed)_2(heedH_2)_2](ClO_4)_4$ (**3**), $[Mn^{II}_2Mn^{IV}_2O_2(heed)_2(MeCN)_2(H_2O)_2(bpy)_2](ClO_4)_4$ (**4**) and $[Mn^{II}_2Mn^{IV}_2O_2(heed)_2(bpy)_2Br_4]\cdot2MeOH$ (**5**·2MeOH). Clusters **1–5** are constructed from the tripodal ligand *N*,*N*-bis(2-hydroxyethyl)ethylene diamine ($heedH_2$) and represent rare examples of tetranuclear Mn clusters possessing the linear *trans* zig-zag topology, being the first $Mn^{II/IV}$ mixed-valent clusters of this type. The molecular clusters can then be used as building blocks in tandem with the (linear) linker dicyanamide ($[N(CN)_2]^-$, dca^-) for the formation of a novel extended network $\{[Mn^{II}_2Mn^{IV}_2O_2(heed)_2(H_2O)_2(MeOH)_2(dca)_2]Br_2\}_n$ (**6**), which exhibits a rare form of the 2D herring bone topology.

Introduction

In recent years enormous research activity in the field of manganese cluster chemistry has been witnessed, partly because of their relevance to the Mn_4 complex at the water oxidation centre of photosystem II, and partly because some of them behave as nanoscale magnets. The discovery that a single molecule could behave like a tiny magnet was a major scientific breakthrough with widespread potential technological implications in high-density information storage and quantum computing. Single-molecule magnets (SMMs) represent the smallest possible magnetic devices and thus a molecular (or bottom-up) and hence controllable approach to nanoscale magnetism, where the energy barrier to magnetisation re-orientation is derived from the anisotropy of the molecular spin rather than the movement of domain walls, as in bulk magnets. The main requirements for observing such behaviour in molecules are a high spin ground state, S, and a significant negative zero-field splitting (D) of that ground state. The upper limit of the energy barrier (U) for the re-orientation (reversal, relaxation) of the magnetisation vector is given by $S^2|D|$ and $(S^2\text{-}1/4)|D|$, for integer and half-integer S values, respectively, and its magnitude, at least in part, controls the temperature below which magnetic hysteresis and bistability are observed.[1] The ability of Mn to exist in a variety of oxidation states makes it a popular choice for SMM synthesis since even antiferromagnetic exchange in mixed-valent clusters is likely to lead to molecules with non-zero spin ground states and the presence of Mn(III) ions guarantees a suitable source of single-ion anisotropy.[1]

The specific design and synthesis of tetranuclear Mn clusters, although of interest from a spin frustration perspective, has mainly been pursued in order to make models for the complex responsible for the oxidation of water in the oxygen evolving centre (OEC) of Photosystem II (PSII) in green plants and cyanobacteria.[2] Recent crystallographic[3] and polarised EXAFS studies[4] on the PSII reaction centre of *Thermosynechococcus elongatus* confirm the cluster to be an oxide-bridged $[Mn_4Ca]$ complex with (mainly) peripheral carboxylate ligation.

The most common $[Mn_4]$ complexes in the literature possess $[Mn_4O_2]$ 'butterfly' cores, which are best described as consisting of two fused or vertex-sharing $[Mn_3(\mu_3\text{-}O)]$ triangles (Fig. 1).[5] Less common is the $[Mn_4O_4]$ cubane topology where the Mn centres occupy the four alternate corners of a cube (Fig. 1);[6] and less

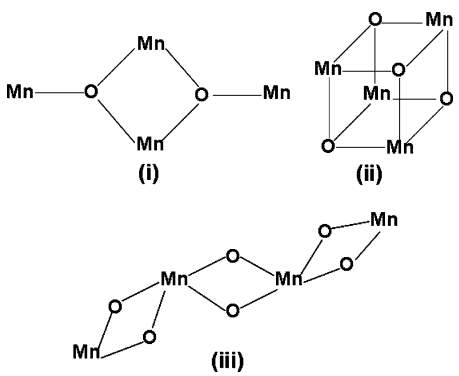

Fig. 1 Schematic showing the common tetranuclear $[Mn_4O_2]$ 'butterfly' (i) and $[M_4O_4]$ cubane (ii) topologies and the rare linear *trans* zig-zag topology (iii) observed in **1–6**.

[a]*School of Chemistry, Joseph Black Building, West Mains Road, Edinburgh, UK EH9 3JJ. E-mail: ebrechin@staffmail.ed.ac.uk; Tel: +44 (0)131 650 7545*
[b]*Laboratory of Inorganic Chemistry, Department of Chemistry, National and Kapodistrian University of Athens, Athens, Greece.*
[c]*CNR-INFM Nat. Res. Center, Dept. of Physics, University of Modena and Reggio Emilia, Modena, Italy.*

† Dedicated to Prof. Keith Murray on the occasion of his 65th birthday.

‡ Electronic supplementary information (ESI) available: Figures and Tables illustrating the H-bonding interactions, distances and angles. CCDC reference numbers 682648–682653. For ESI and crystallographic data in CIF or other electronic format see DOI: 10.1039/b804897e

common still are those with a linear zig-zag arrangement which may take either a *cis* or (much rarer) *trans* conformation (Fig. 2).[7]

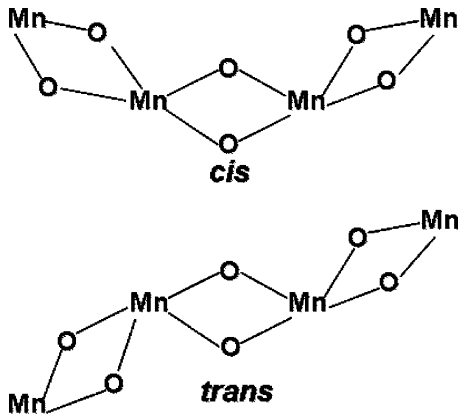

Fig. 2 Schematic illustrating the *cis* and *trans* structural conformers of tetranuclear Mn complexes with a linear $[Mn_4O_6]$ core.

For some years we have been building SMMs with tripodal alcohol ligands of general formula R–C$(CH_2OH)_3$ (where R = H, CH_3, Et *etc*) and their many derivatives (Scheme 1).[8] A natural extension to these studies is the investigation of the coordination chemistry of analogous organic molecules in which one (or more) of the alcohol 'arms' is replaced by an alternative functional group(s), for example an amine group. While each alkoxide arm has the potential to bridge up to three metals (and thus a maximum of seven metals per tripodal ligand), the $–NH_2$ 'arm' is likely, if bonded, to act solely as a monodentate/terminal capping unit and should give rise to a number of related, yet different, structural topologies.[8] We herein report our initial investigations into the reactivity of *N*,*N*-bis(2-hydroxyethyl)ethylene diamine ($heedH_2$); a relatively unexplored ligand whose chemistry is thus far restricted to the dimeric complexes $[Cu_2(heedH)_2](PF_6)_2$[9] and $[Zn_2(\mu_2\text{-}O)(heedH_2)](BF_4)_2$.[10]

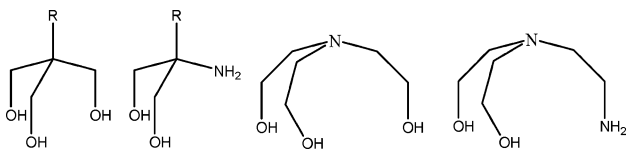

Scheme 1 Structures of R–C$(C_2H_4OH)_3$ (R=CH_3, H_3thme; R = CH_3CH_2, H_3tmp); R–C$(CH_2OH)_2NH_2$ (R = CH_3, $ampH_2$; R = CH_3CH_2, $aepH_2$); triethanolamine, H_3tea; and $heedH_2$, shown from left to right.

Results and discussion

The reaction of $Mn^{II}X_2$ salts (X = Br, Cl, ClO_4) in the presence of the tripodal ligand $heedH_2$ in suitable solvents (MeOH, EtOH or MeCN) has produced a family of tetranuclear mixed valent Mn complexes: $[Mn^{II}_2Mn^{IV}_2O_2(heed)_2(EtOH)_6Br_2]Br_2$ (**1**), $[Mn^{II}_2Mn^{IV}_2O_2(heed)_2(H_2O)_2Cl_4]$ (**2**), $[Mn^{II}_2Mn^{IV}_2O_2(heed)_2(heedH_2)_2](ClO_4)_4$ (**3**), $[Mn^{II}_2Mn^{IV}_2O_2(heed)_2(MeCN)_2(H_2O)_2(bipy)_2](ClO_4)_4$ (**4**), $[Mn^{II}_2Mn^{IV}_2O_2(heed)_2(bipy)_2Br_4]$ (**5**); and a 2D network of tetranuclear $Mn^{II/IV}$ clusters $\{[Mn^{II}_2Mn^{IV}_2O_2(heed)_2(H_2O)_2(MeOH)_2(dca)_2]Br_2\}_n$ (**6**). This family represents only the second example of Mn complexes exhibiting the linear zig-zag *trans* topology, first seen in the compound $[Mn^{II}_4(H_2L3)_2(OAc)_2(py)_5]$ (where H_2L3 = 2-hydroxy-1,3-bis[3-(2-hydroxyphenyl)-3-oxopropionyl]benzene),[11] and are the first to exhibit a $[Mn^{II}_2Mn^{IV}_2]$ mixed-valent charge distribution. **1–6** are isostructural, comprising identical $\{Mn_4O_6\}$ cores and differ only in their terminal ligation at the peripheral Mn^{II} sites. For this reason we will restrict our discussion to complex **1**, highlighting any differences.

Reaction of anhydrous $MnBr_2$ with $heedH_2$ in EtOH produces the complex $[Mn^{II}_2Mn^{IV}_2O_2(heed)_2(EtOH)_6Br_2]Br_2$ (**1**) which crystallises in the monoclinic space group $P2_1/c$ (Table 1).‡§ The core of the complex consists of a linear zig-zag arrangement of four Mn ions (Fig. 3), with charge balance considerations, bond valence sum (BVS) calculations and analysis of the bond lengths (Table 2 and ESI‡) showing that the two outer Mn ions (Mn2 and s.e (symmetry equivalent)) are in the II+ oxidation state and the two central Mn ions (Mn1 and s.e) are in the IV+ oxidation state. The two central Mn^{IV} ions are linked *via* two symmetry equivalent $\mu\text{-}O^{2-}$ ions (O1) with an inversion centre lying at the midpoint between O1 and O1′ (Fig. 3). The tripodal $heed^{2-}$ ligands are doubly deprotonated lying above and below the Mn1 ··· Mn1′ plane, bonding terminally to the central Mn^{IV} centres through their N atoms (Mn1–N11 = 2.089(2), and Mn1–N231 = 2.053(2) Å), while the two alkoxide arms (O331 and

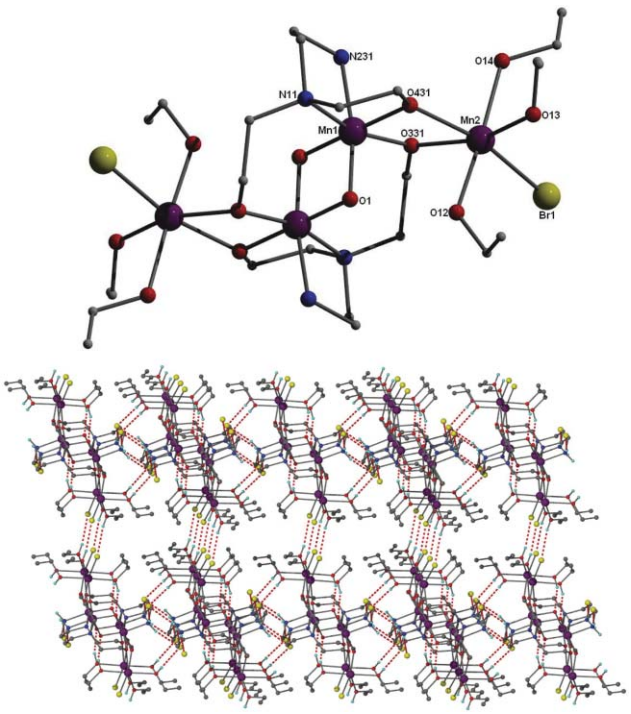

Fig. 3 Molecular structure of $[Mn_4O_2(heed)_2(EtOH)_6Br_2]Br_2$ (**1**, top), H atoms and Br^- anions omitted for clarity. Selected bond lengths (Å): Mn1–O1 = 1.816(2), Mn1–N11 = 2.089(2), Mn1–N231 = 2.053(2), Mn2–Br1 = 2.5716(5), Mn2–O331 = 2.189(2) and Mn2–O431 = 2.142(2). The packing of the layers in **1** demonstrating the brickwall arrangement of the $[Mn_4]$ clusters (bottom).

§ All manipulations were performed under aerobic conditions, using materials as received. **CAUTION!** Although no problems were encountered in this work, care should be taken when using the potentially explosive perchlorate anion.

Table 1 Crystallography data obtained for **1–6**

	1	**2**·2EtOH·H_2O	**3**	**4**	**5**·2MeOH	**6**
Fomula	$C_{24}H_{64}N_4O_{12}Br_4Mn_4$	$C_{12}H_{32}N_4O_8Cl_4Mn_4$	$C_{24}H_{60}N_8O_{26}Cl_4Mn_4$	$C_{36}H_{54}N_{10}O_{24}Cl_4Mn_4$	$C_{34}H_{52}N_8O_8Br_4Mn_4$	$C_{10}H_{24}N_5O_6Br_1Mn_2$
Formula weight/g mol^{-1}	1140.12	1112.48	1238.30	1431.46	1240.16	500.09
Crystal system	Monoclinic	Trigonal	Monoclinic	Triclinic	Triclinic	Monoclinic
Space group	$P21/c$	$R\bar{3}$	$P21/c$	$P\bar{1}$	$P\bar{1}$	$P21/c$
a/Å	13.6721(3)	23.5608(3)	11.1558(10)	9.8751(3)	9.1916(3)	14.6719(4)
b/Å	9.1130(2)	23.5608(3)	10.9531(10)	13.9986(4)	9.4296(3)	10.8780(3)
c/Å	17.2367(4)	15.5896(6)	18.8477(10)	14.1558(4)	14.1811(5)	14.9952(4)
α/°	90	90	90	63.722(2)	103.468(2)	90
β/°	99.485	90	100.282(10)	73.229(2)	90.430(2)	113.4910(10)
γ/°	90	120	90	78.714(2)	111.896(2)	90
V/Å^3	2118.23(8)	7494.6(3)	2266.0(3)	1674.73(9)	1103.01(7)	2194.90(10)
Z	2	9	2	1	1	4
ρ_{calcd}/g cm^{-3}	1.787	1.497	1.815	1.361	1.867	1.51
T/K	150	150	150	150	150	150
λ/Å	0.7103	0.71073	0.71073	0.71073	0.71073	0.71073
μ/mm^{-1}	4.991	1.854	1.422	0.973	4.798	3.000
Independent reflections (R_{int})	25247/5196 (0.043)	33942/4268 (0.025)	55249/13087 (0.039)	21077/9231 (0.043)	24353/6465 (0.036)	26611/5814 (0.033)
Observed reflections [$I>2\sigma(I)$]	3655	3261	11011	6997	5134	4369
R_1	0.0308	0.0378	0.0460	0.0701	0.0317	0.0483
wR_2	0.0699	0.1062	0.1000	0.1755	0.0800	0.1389
GOF on F^2	0.7442	0.9935	0.9051	0.9925	0.9266	0.9159
$\Delta\rho_{max,min}$/e Å^{-3}	1.23–0.91	1.04–0.53	1.46–1.54	1.22–0.94	1.05–0.93	3.27–0.57

Table 2 Bond lengths (Å) and angles (°) for **1–6**

1		**2**		**3**	
Mn1–O1	1.8158(18)	Mn1–N11	2.097(2)	Mn1–O422	2.0949(14)
Mn1–N11	2.089(2)	Mn1–O12′	1.8384(18)	Mn1–O412′	2.2294(14)
Mn1–N231	2.053(2)	Mn1–N21	2.049(2)	Mn1–O411	2.1815(17)
Mn1–O431	1.5134(18)	Mn1–O41	1.8978(18)	Mn1–O421	2.2005(16)
Mn1–O331′	1.8719(18)	Mn1–O61	1.8796(17)	Mn1–N11	2.3987(19)
Mn1–O1′	1.8280(17)	Mn1–O12	1.8186(17)	Mn1–N431	2.212(2)
Mn2–O13	2.188(2)	Mn2–O41	2.1470(18)	Mn2–O1	1.8149(13)
Mn2–O14	2.2196(19)	Mn2–O61	2.1659(18)	Mn2–O1′	1.8209(14)
Mn2–O12	2.221(2)	Mn2–C113	2.3929(8)	Mn2–O422	1.9131(14)
Mn2–Br1	2.5716(5)	Mn2–C114	2.4364(8)	Mn2–O412′	1.8681(14)
Mn2′–O431	2.1421(19)	Mn2–O15	2.090(2)	Mn2–N12	2.0987(17)
Mn2–O331	2.1877(18)			Mn2–N432	2.0556(18)
Mn1′–O1–Mn1	96.18(8)	Mn2–O61–Mn1	103.96(8)	Mn2′–O1–Mn2	95.95(6)
Mn1–O331–Mn2	102.51(8)	Mn1′–O12–Mn1	96.89(8)	Mn1′–O412–Mn2′	101.42(6)
Mn2′–O431–Mn1	102.79(8)	Mn2–O41–Mn1	104.04(8)	Mn1–O422–Mn2	104.90(6)
4		**5**		**6**	
Mn1–O9′	1.882(3)	Mn1–O23′	1.8667(16)	Mn1–O13′	1.819(2)
Mn1–O6	1.512(3)	Mn1–O27′	1.8070(16)	Mn1–O6	1.905(2)
Mn1–O29′	1.831(2)	Mn1–O20	1.9211(17)	Mn1–O9	1.865(2)
Mn1–O29	1.817(2)	Mn1–O27	1.8212(16)	Mn1–O13	1.820(2)
Mn1–N3	2.089(3)	Mn1–N17′	2.100(2)	Mn1–N3	2.093(3)
Mn1–N12	2.047(3)	Mn1–N26	2.068(2)	Mn1–N12	2.071(3)
Mn2–O28	2.201(3)	Mn2–Br3	2.6723(4)	Mn2–O14	2.215(3)
Mn2–N14	2.236(3)	Mn2–Br4	2.6372(4)	Mn2–O16	2.211(3)
Mn2–N24	2.236(3)	Mn2′–N10	2.254(2)	Mn2–N23	2.148(4)
Mn2–N25	2.211(4)	Mn2–N12	2.278(2)	Mn2–N18	2.161(4)
Mn2–N25	2.211(4)	Mn2–N12	2.278(2)	Mn2–N18	2.161(4)
Mn1′–O29–Mn1	96.15(11)	Mn1–O27–Mn1′	96.15(7)	Mn1–O13–Mn1′	96.44(11)
Mn2–O6–Mn1	102.86(12)	Mn2–O20–Mn1	105.66(7)	Mn2–O6–Mn1	104.13(11)
Mn2′–O9–Mn1′	101.42(12)	Mn2′–O23–Mn1	102.54(7)	Mn2–O9–Mn1	102.36(10)

O431) bridge the central Mn^{II} ions to the outer Mn^{IV} ions. Each metal centre exhibits distorted octahedral geometry with the coordination spheres at the peripheral Mn^{II} sites completed by terminal Br^- ions (Br1) and EtOH molecules. The resultant $[Mn_2^{II}Mn_2^{IV}O_2(heed)_2(EtOH)_6Br_2]^{2+}$ cation is charge balanced by the presence of two Br^- anions (Br2 and s.e) which 'link' the $[Mn_4]$ clusters through H-bonding to their NH_2 protons (N231–H23 $\cdots$ Br2 = 3.483 Å, N231–H4 $\cdots$ Br2 $[1-x, 0.5+y, 1.5-z]$ = 3.491 Å) and terminal EtOH ligands (O14–H28 $\cdots$ Br2 $[x, 1.5-y, -0.5+z]$ = 3.275 Å) to form layers running parallel to the *bc* plane (Fig. S1, Table S1‡). Those layers are further bridged through two complementary H-bonds that involve the second EtOH molecule and the terminal Br^- ions (O13–H24 $\cdots$ Br1 $[2-x, 2-y, 1-z]$ = 3.234 Å). The third EtOH molecule forms an *intramolecular* H-bond with one μ-O^{2-} ion. The (numerous) intermolecular H-bonding interactions lead to the individual $[Mn_4]$ clusters packing in the common brickwall formation in the crystal (Fig. 3).

The same reaction using $MnCl_2{\cdot}6H_2O$ produces the analogous complex $[Mn^{II}_2Mn^{IV}_2(heed)_2(H_2O)_2Cl_4]{\cdot}2EtOH{\cdot}H_2O$ (**2**·2EtOH·H_2O). **2** (Fig. 4) crystallises in the rhombohedral $R\bar{3}$ space group and differs from **1** only in that it contains four terminally bound Cl^-ions and two H_2O molecules on the peripheral Mn^{II} ions instead of two halides and six solvent molecules. The result is a neutral complex. Numerous H-bonding interactions are observed between the discrete $[Mn_4]$ molecules,

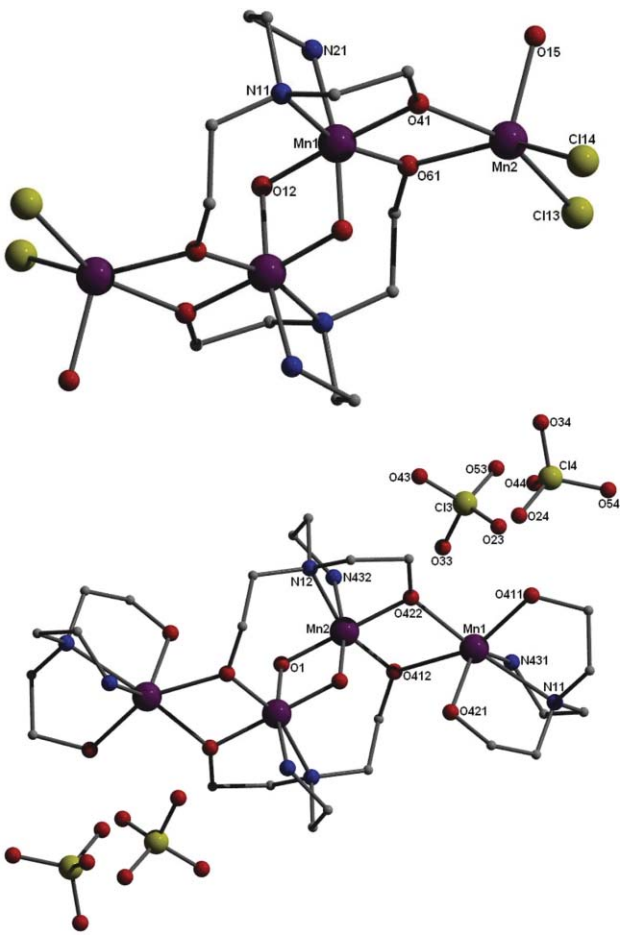

Fig. 4 Molecular structures of $[Mn_4O_2(heed)_2(H_2O)_2Cl_4]$ (**2**, top) and $[Mn_4O_2(heed)_2(heedH_2)_2](ClO_4)_4$ (**3**, bottom).

primarily forged by the four terminal Cl^- ligands (Cl3 and Cl4). Both interact with protons from two nearby $heed^{2-}$ (NH_2) protons (N21–H21 $\cdots$ Cl13 $[1/3+y, 2/3-x+y, 2/3-z]$ = 3.308, N21–H22 $\cdots$ Cl14 $[1/3-x+y, 2/3-x, -1/3+z]$ = 3.315 Å) on two neighbouring $[Mn_4]$ units. A strong H-bond is also formed between the μ-bridging O^{2-} ion (O12 and s.e) situated at the centre of the $[Mn^{II}_2Mn^{IV}_2O_6]$ core and the terminal H_2O molecule of an adjacent cluster (O15–H15 $\cdots$ O12 $[1/3+x-y, -1/3+x, 2/3-z]$ = 2.601 Å), which in turn is also H-bonded to a neighbouring Cl^- ligand (O15–H16 $\cdots$ Cl14 $[1/3-x+y, 2/3-x, -1/3+z]$ = 3.140 Å). In this arrangement each $[Mn_4]$ unit is H-bonded to four other $[Mn_4]$ units *via* 16 H-bonds (Fig. S2‡) giving rise to a three dimensional (3D) framework which adopts the sod topology[12–14] (Fig. 5) with Schlafli symbol 4^26^4. Hexagonal channels with *ca.* 9 Å diameter running along the *c* axis are formed within the 3D framework of **2** (Fig. 5).

Using $Mn^{II}(ClO_4){\cdot}6H_2O$ removes the availability of terminal ligands (*i.e.* Hal^-) and gives rise to the formation of the complex $[Mn^{II}_2Mn^{IV}_2O_2(heed)_2(heedH_2)_2](ClO_4)_4$ (**3**, Fig. 4). Although the $\{Mn^{II}_2Mn^{IV}_2O_6\}$ core remains identical, the peripheral ligation is markedly different. The four $heed^{x-}$ ligands (two crystallographically unique pairs) in **3** appear in two different levels of deprotonation, which leads to different bonding motifs. As in **1** and **2**, two doubly deprotonated $heed^{2-}$ ligands sit above and below the central $Mn^{IV} \cdots Mn^{IV}$ plane using their $=N–CH_2CH_2O^-$ arms to bridge the outer Mn^{II} ions to the central Mn^{IV} centres. The second type remain neutral ($heedH_2$) and face-cap the outer Mn^{II} ions through their N atoms (N431 and N11) and their alcohol arms (O411 and O421) (Fig. 4). The $[Mn^{II}_2Mn^{IV}_2O_2(heed)_2(heedH_2)_2]^{4+}$ complex is charge balanced by four ClO_4^- counter ions (two symmetry related pairs) linked to the tetranuclear cluster *via* H-bonding interactions with the OH and NH_2 protons on the capping $heedH_2$ and bridging $heed^{2-}$ arms of the tripodal ligands. This intermolecular H-bonding between the clusters and the perchlorates in **3** creates a 2D layer running parallel to the *ab* plane (Fig. S3‡). The layers are connected to the third dimension *via* weaker H-bonds that involve the perchlorate oxygen atoms and alkyl protons of $heed^{2-}$ ligands on adjacent $[Mn_4]$ moieties.

Introduction of the chelating ligand 2,2-bipyridine (bpy) to the general reaction scheme, expands this family further with the formation of the similar complexes $[Mn^{II}_2Mn^{IV}_2O_2(heed)_2(bpy)_2(MeCN)_2(H_2O)_2](ClO_4)_4$ (**4**) and $[Mn^{II}_2Mn^{IV}_2O_2(heed)_2(bpy)_2Br_4]$ (**5**, Fig. 6), which crystallises in the same crystal system and space group. The $\{Mn^{II}_2Mn^{IV}_2O_6\}$ core remains intact in both cases and differ to their siblings only in the presence of two chelating bpy ligands capping the ends of the $[Mn_4]$ complexes at the Mn^{II} sites. The remaining coordinating sites at the Mn^{II} ions are occupied by terminal MeCN and H_2O ligands in **4**, and four terminal Br^- ions in **5**.

The clusters of **4** form H-bonded chains along the *a* axis, which involve one hydrogen atom of the terminal H_2O molecules, one NH_2 proton of the $heed^{2-}$ ligand and one of the two crystallographically independent ClO_4^- anions (O28–H282 $\cdots$ O39 = 2.966 Å, N12–H122 $\cdots$ O38 $[1+x, y, z]$ = 3.027 Å) (Fig. S4‡). The second crystallographically independent ClO_4^- anion is H-bonded to a $[Mn_4]$ cluster *via* a single H-bond. These linear chains of **4** pack in parallel rows along the *b* axis due to intermolecular π–π stacking interactions ($\pi_{centroid} \cdots \pi_{centroid}$ = 3.605 Å and 3.775 Å) between the

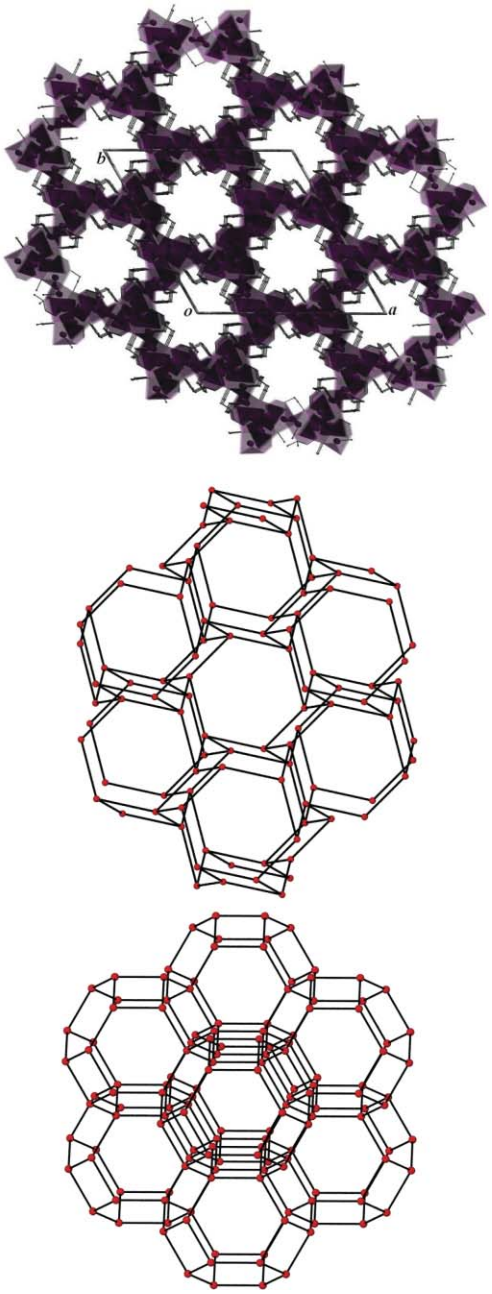

Fig. 5 $R\bar{3}$ packing motif in **2** shown down the *c* axis. H atoms have been omitted for clarity and the $\{MnO_4N_2\}$ polyhedra are shaded in purple (top). The sod network adopted by **2** (middle) and the ideal sod net (bottom).

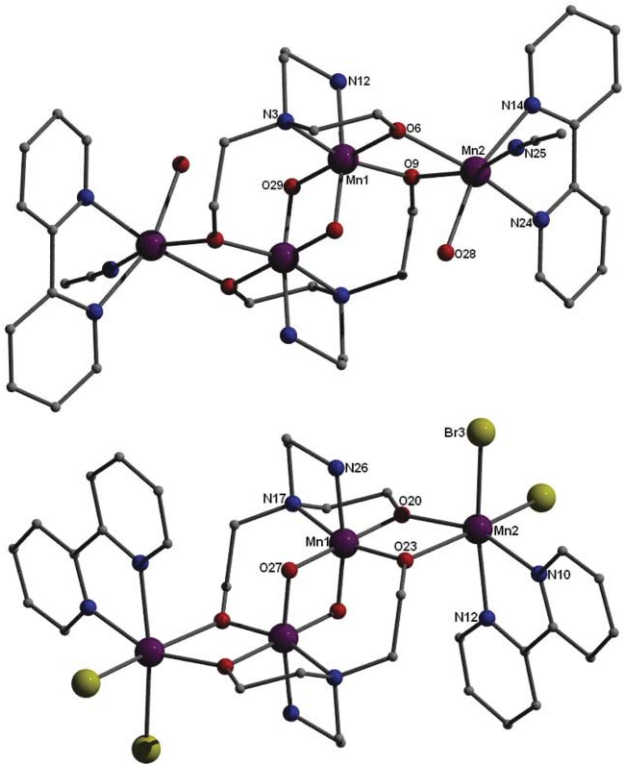

Fig. 6 Molecular structures of $[Mn_4O_2(heed)_2(MeCN)_2(H_2O)_2(bpy)_2]$ (**4**) (top) and $[Mn_4O_2(heed)_2(bpy)_2Br_4]$ (**5**) (bottom).

chelating bpy ligands forming a 2D layer parallel to the *ab* plane (Fig. S5‡).

The $[Mn_4]$ clusters in **5** are also arranged in H-bonded chains running along the *b* axis, which involve the terminal Br^- ions (Br3) and the hydrogen atoms of the NH_2 groups of the $heed^{2-}$ ligands of adjacent $[Mn_4]$ clusters (N26–H261 $\cdots$ Br3 = 3.567 Å, N26–H262 $\cdots$ Br3 $[-x, 2-y, 1-z]$ = 3.521 Å), forming $R_2^2(8)$ rings (Fig. S6‡). The MeOH solvent molecule of crystallisation in **5** hydrogen bonds to the other terminal Br^- ion (Br4) at a distance of 3.276 Å (O29–H291 $\cdots$ Br4). Akin to **4**, the $[Mn_4]$ chains in **5** interact through π–π stacking interactions ($\pi_{centroid} \cdots \pi_{centroid}$ = 3.789 Å) to form a layer parallel to the *bc* plane (Fig. S7‡). Weaker H-bonding interactions stabilise the packing of the molecules in the crystal. Those interactions involve the Br^- ions and both the aromatic bpy protons and the aliphatic protons of the alkyl arms of the $heed^{2-}$ ligands on neighbouring $[Mn_4]$ clusters.

The presence of terminal halide ions and solvent molecules in complexes **1**, **2** and **5** alerted us to the possibility of replacing these with (linear) connector ligands in order to introduce 1, 2 or 3 dimensionality. The linking of paramagnetic clusters into such arrays may provide new and important insights into the transition from purely molecular magnetic properties to long range 1, 2 and 3D bulk magnetic order. Furthermore, the ordering or templating of such paramagnetic systems may eventually form the basis for commercial fabrication of arrays of such magnetic materials.[15] To this end, the reaction of anhydrous $MnBr_2$, $heedH_2$ and sodium dicyanamide (Na(dca); $NaN(CN)_2^-$) produces $[\{Mn^{II}_2Mn^{IV}_2O_2(heed)_2(H_2O)_2(MeOH)_2(dca)_2\}Br_2]_n$ (**6**, Fig. 7–9). The $[Mn^{II}_2Mn^{IV}_2O_6]$ core in **6** is isostructural to its siblings and coordination at the peripheral Mn^{II} sites (Mn2) is completed by two H_2O and EtOH ligands and four dca^- ligands, which occupy two equatorial positions at each Mn^{II} centre (Fig. 7).

As observed in numerous dca based 1, 2 and 3D extended networks comprising monometallic nodes,[16] each dca^- ligand then bridges to another $[Mn^{II}_2Mn^{IV}_2]$ cluster to form a 2D sheet with a [4,4] grid-like topology (Fig. 9c). More specifically, the 2D network in **6** joins a small family of extended networks possessing a rare form of the 2D herring bone topology (Fig. 9a).[17–20] The more familiar 2D herring bone motif comprises 3-connector nodes

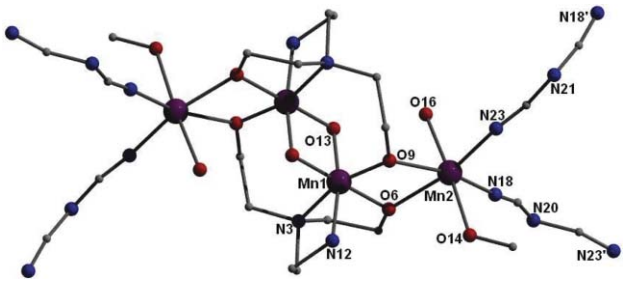

Fig. 7 Structure of the $[Mn^{II}_2Mn^{IV}_2O_2(heed)_2(EtOH)_2(H_2O)_2(dca)_2]Br_2$ building block in **6**. Br^- ions and H-atoms have been omitted for clarity.

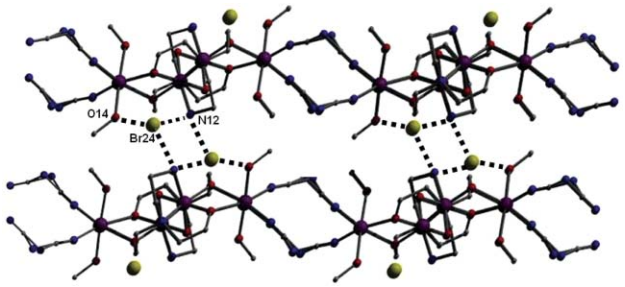

Fig. 8 H-bonding interactions (dashed lines) linking the 2D sheets in **6**.

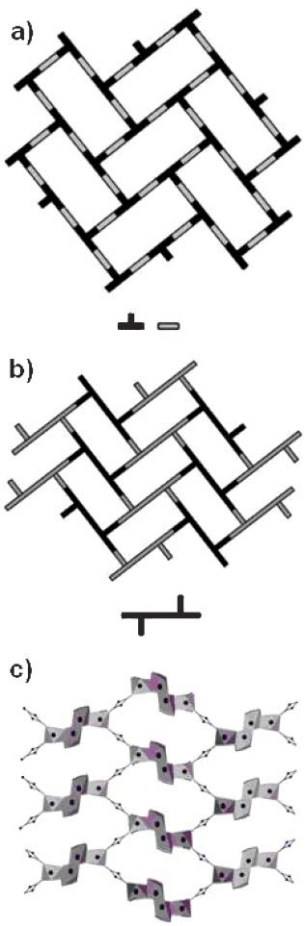

Fig. 9 Schematic illustrating (a) the common herring bone 2D topology built from 3-connector 'T' shaped nodes (inset). (b) The much rarer version of this topology comprised of $[Mn^{II}_2Mn^{IV}_2]$ building blocks (inset). (c) Crystal structure of the actual 2D herring bone topology observed in **6**.

linked by linear spacer ligands (Fig. 9a), however we may best describe the connectivity in **6** by thinking of the $[Mn^{II}_2Mn^{IV}_2O_6]$ moieties as two fused 'T' shaped 3-connector nodes, which link to give our 2D extended network (Fig. 9b and Fig. 9c).

The 2D sheets in **6** lie in the *ab* plane and propagate along the *c* axis to form an angle of approximately 30° with the *ab* plane, with respect to the cell origin. These planar sheets then stack in an off-set fashion along the *c* axis. The Br^- anions sit in between the 2D sheets (Fig. 8) and are "locked" there by three H-bonding interactions. Two H-bonds arise from the lower 2D layer *via* a hydroxyl proton from a terminal MeOH ligand (O14–H142 $\cdots$ Br24 $[-x, 1/2 + y, 1/2 - z] = 3.250$ Å) and a NH_2 proton from one amine arm of a $heed^{2-}$ ligand (N12–H122 $\cdots$ Br24 $[-x, 1/2 + y, 1/2 - z] = 3.570$ Å). The third and final H-bond is formed *via* a NH_2 proton from a symmetrically equivalent $heed^{2-}$ arm belonging to the upper 2D sheet (N12–H121 $\cdots$ Br24 = 3.621 Å). The second MeOH molecule forms an *intramolecular* H-bond with one μ-O^{2-} ion (O16–H162 $\cdots$ O13 $[-x, 2 - y, 1 - z] = 2.736$ Å). Each $[Mn_4]$ is H-bonded to two Br^- ions below the layer and to two Br^- ions above the layer. Therefore, each $[Mn_4]$ connects to four other $[Mn_4]$ moieties *via* the Br^- links. In this arrangement each $[Mn_4]$, which is connected to four other $[Mn_4]$ clusters through the dca^- anions, is also attached to four other $[Mn_4]$ clusters *via* the the H-bonded Br^- links. Therefore, each $[Mn_4]$ cluster serves as an 8-connected node within the resultant framework which adopts the bcu topology[13,14,21] with Schlafli symbol $4^{24}6^4$ (Fig. 10).

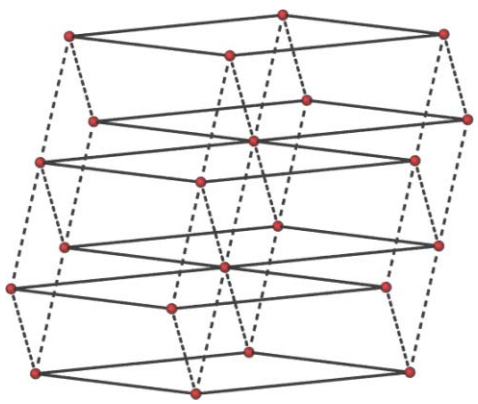

Fig. 10 The 3D 8-connected bcu net adopted by **6**. Solid lines represent the connections through the dca anions while dashed lines represent the H-bonded links.

Magnetic studies

DC magnetic susceptibility studies were carried out on crystalline samples of **1–6** in the 4–300 K temperature range in an applied field of 0.1 T. The behaviour of **1–6** is essentially identical (within this temperature range) and so here we limit our discussion to complex **1**. The room temperature value of $\chi_m T$ in **1** (Fig. 11) is slightly lower (10.67 $cm^3\ mol^{-1}\ K$) than the expected value of ~12.5 $cm^3\ mol^{-1}\ K$ for four non-interacting Mn ions (2 × Mn^{II}, 2 × Mn^{IV}), indicative of dominant antiferromagnetic exchange between the metal centres. $\chi_m T$ then slowly decreases with temperature before dropping more abruptly at approximately 125 K, reaching a value of 3.36 $cm^3\ mol^{-1}\ K$ at 4 K. Simulation of the data using the $2 - J$ model described in Scheme 2 and spin

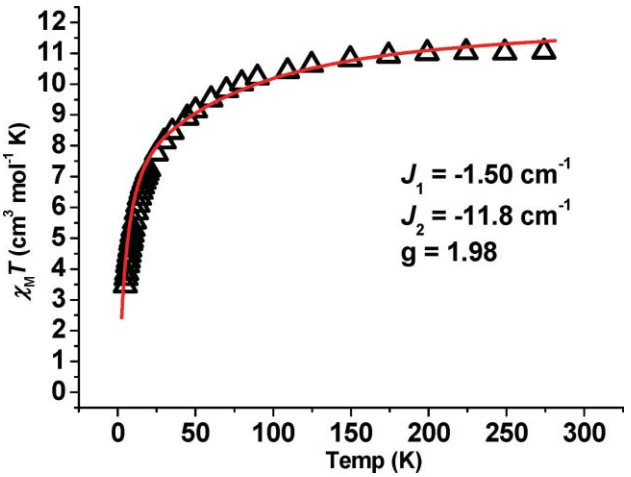

Fig. 11 Plot of $\chi_m T$ *vs.* T obtained for **1** (Δ) along with the best-fit (solid red line) affording the spin Hamiltonian parameters $J_1 = -1.50\ \text{cm}^{-1}$, $J_2 = -11.8\ \text{cm}^{-1}$ and $g = 1.98$.

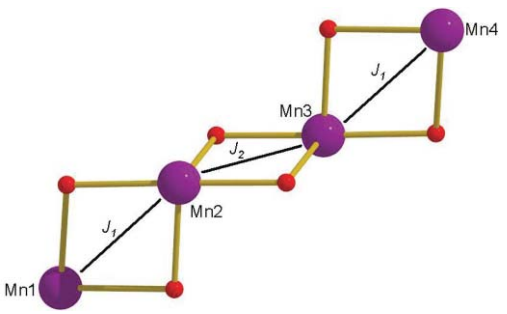

Scheme 2 The exchange interaction scheme employed for **1**.

Hamiltonian eqn (1) afforded the parameters $S = 0$, $g = 1.98$, $J_1 = -1.50\ \text{cm}^{-1}$ and $J_2 = -11.8\ \text{cm}^{-1}$.[22] The 1st ($S = 1$) and 2nd ($S = 2$) excited states lie just 0.32 and 1.01 cm^{-1} above the $S = 0$ ground state, explaining the relatively large value of 3.36 $\text{cm}^3\ \text{mol}^{-1}$ K observed at 4 K.

$$\mathscr{H} = -2J_1(\hat{S}_1 \cdot \hat{S}_2 + \hat{S}_3 \cdot \hat{S}_4) - 2J_2(\hat{S}_2 \cdot \hat{S}_3) \quad (1)$$

Detailed field-dependent heat capacity experiments were conducted for **6** (Fig. 12). The first striking feature is a λ-type anomaly observed at $T = 3$ K, having a relative height of $\sim 1.2R$. Because its position and height are insensitive to the applied field (Fig. 12a) and there is no counterpart in the magnetic susceptibility (Fig. S8‡), we conclude that this anomaly is of non-magnetic origin, and likely associated with a structural transition. At much lower temperatures, a second sharp peak occurring at $T_N = 0.72$ K reveals the onset of a phase transition[23], whose magnetic origin is proven by the fact that it is completely removed by applying fields of sufficient intensity (Fig. 12a). One can notice though that it is hardly affected by the relatively large field $B_0 = 1$ T, suggesting the transition is to an antiferromagnetically ordered state. To get a deeper understanding of the magnetic ordering, we estimate the magnetic contribution C_m. Noting that fields higher than ~ 5 T are enough to shift any magnetic contribution well above 2 K (Fig. 12a), we obtain C_m by subtracting the experimental specific heat measured for $B_0 = 7$ T to the total zero-field specific heat C. The result is depicted in Fig. 12b, together with the curve obtained similarly for $B_0 = 1$ T.

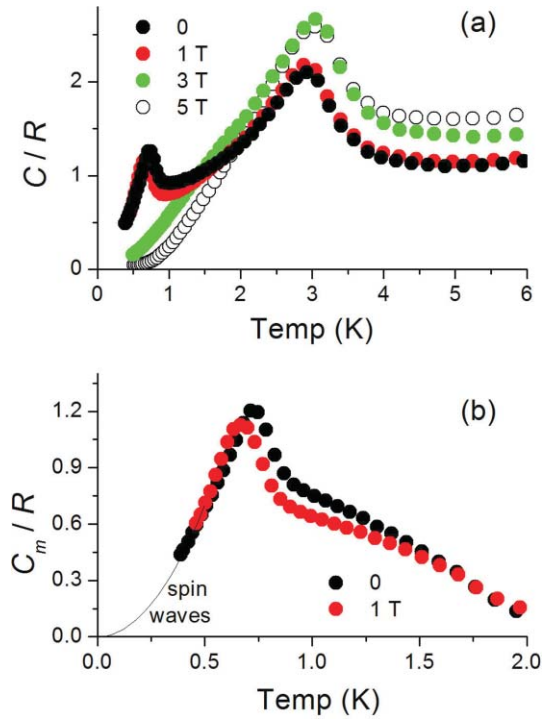

Fig. 12 (a) Plot of the experimental specific heat C normalised to the gas constant R in the indicated temperature and field ranges. (b) Low temperature magnetic contribution C_m to the specific heat. The solid line is the calculated contribution associated with spin-wave excitations.

The long tail above T_N reflects the presence of magnetic correlations, probably existing within the 2D extended networks. At the lowest temperatures, the experimental specific heat displays a T^2 dependence, $C_m \propto AT^2$ with $A \cong 23\ \text{mJ K}^{-3}\ \text{mol}^{-1}$, suggesting the existence of 2D spin waves with a linear dispersion relation. Finally, the estimate of the zero-field magnetic entropy content $\Delta S_m/R = \int C_m/(RT)\text{d}T$ provides a curve tending at higher T to the value of $\sim 1.5R$. The latter is close to the value of the magnetic entropy $R\ln(2S+1) = 1.61R$, expected for spin $S = 2$, in agreement with the dc susceptibility data that showed that both $S = 1$ and $S = 2$ states are within just 1 cm^{-1} of the $S = 0$ ground state.

Conclusions

Initial investigations into the coordination chemistry of the unexplored tripodal ligand *N*,*N*-bis(2-hydroxyethyl)ethylene diamine ($\text{heed}H_2$) has produced a series of mixed-valent $Mn^{II/IV}$ complexes $[Mn^{II}_2Mn^{IV}_2O_2(\text{heed})_2(\text{EtOH})_6Br_2]Br_2$ (**1**), $[Mn^{II}_2Mn^{IV}_2O_2(\text{heed})_2(H_2O)_2Cl_4]\cdot 2\text{EtOH}\cdot H_2O$ (**2**), $[Mn^{II}_2Mn^{IV}_2O_2(\text{heed})_2(\text{heed}H_2)_2](ClO_4)_4$ (**3**), $[Mn^{II}_2Mn^{IV}_2O_2(\text{heed})_2(\text{MeCN})_2(H_2O)_2(\text{bipy})_2](ClO_4)_4$ (**4**) and $[Mn^{II}_2Mn^{IV}_2O_2(\text{heed})_2(\text{bipy})_2Br_4]\cdot 2\text{MeOH}$ (**5**). Clusters **1**–**5** represent rare examples of tetranuclear $[Mn_4O_6]$ complexes exhibiting the linear zig-zag (*trans*) topology. It is difficult to speculate on the reaction pathways that lead to the formation of these complexes (as is the case with all Mn cluster chemistry) but the fact that each is made from a simple Mn^{2+} salt in combination with fully protonated ligands, and are themselves mixed-valent containing two Mn^{2+} and two Mn^{4+} ions, suggests that it is a complicated mechanism involving

the deprotonation–protonation, structural rearrangement and redox chemistry of many species present in solution. Replacement of the terminal ligands (Br^-, Cl^-) with the linear connector dicyanamide (dca^-) anion results in the formation of the [4,4] grid-like $[\{Mn^{II}_2Mn^{IV}_2O_2(heed)_2(H_2O)_2(EtOH)_2(dca)_2\}Br_2]_n$ (**6**). The structure of **6** comprises a rare form of the 2D sheet-like 'herring bone' topology made up of two fused 'T' shaped 3-connector units, as opposed to the more common 'T' shaped 3-connector moieties observed in standard 2D herring bone architectures. Bulk magnetic susceptibility measurements show dominant but weak antiferromagnetic exchange between the metal centres in the 4–300 K temperature range. The temperature and field dependencies of the heat capacity reveal that (**6**) undergoes a phase transition at 0.7 K to an antiferromagnetically ordered state and has a relatively large amount of low-dimensional magnetic fluctuations at higher temperatures, in agreement with the 2D structure and that the feature observed at 3 K is non-magnetic (structural) in nature. The synthesis of a family of metal clusters whose peripheral ligation can be altered without affecting the magnetic core and their subsequent use in the formation of a novel extended network is encouraging since the tailoring of magnetic building blocks into functional arrays is an exciting perspective.

Experimental

$[Mn_4O_2(heed)_2(EtOH)_6Br_2]Br_2$ (1)

Anhydrous $MnBr_2$ (0.5 g, 2.3 mmol) and $heedH_2$ (0.34 g, 2.3 mmol) were dissolved in 25 cm^3 of EtOH and stirred for 1 h. The solution was then filtered and X-ray quality crystals of **1** were obtained upon slow Et_2O diffusion of the mother liquor in ~42% yield. Elemental analysis (%) calculated for $C_{24}H_{64}N_4O_{12}Br_4Mn_4$: C 25.28, H 5.66, N 4.91. Found: C 24.92, H 5.39, N 4.53.

$[Mn_4O_2(heed)_2(H_2O)_2(Cl)_4]$ (2)

$MnCl_2{\cdot}4H_2O$ (0.4 g, 2 mmol) and $heedH_2$ (0.29 g, 2 mmol) were dissolved in 25 cm^3 of EtOH and stirred for 1 h. X-Ray quality crystals of **2** were obtained in good yield (35%) after slow evaporation of the mother liquor. Elemental analysis (%) calculated for $C_{12}H_{32}N_4O_8Cl_4Mn_4$: C 19.96, H 4.47, N 7.76. Found: C 19.70, H 4.70, N 7.35.

$[Mn_4O_2(heed)_2(heedH_2)_2](ClO_4)_4$ (3)

$Mn(ClO_4)_2{\cdot}4H_2O$ (0.72 g, 2.8 mmol) and $heedH_2$ (0.4 g, 2.8 mmol) were dissolved in 25 cm^3 of MeCN and stirred for 1 h. Upon filtration and Et_2O diffusion, black crystals of **3** were formed in ~40% yield after 2 d. Elemental analysis (%) calculated for $C_{24}H_{60}N_8O_{26}Cl_4Mn_4$: C 23.28, H 4.88, N 9.05. Found: C 23.75, H 4.73, N 9.36.

$[Mn_4O_2(heed)_2(MeCN)_2(H_2O)_2(bpy)_2](ClO_4)_4$ (4)

$Mn(ClO_4)_2{\cdot}6H_2O$ (0.35 g, 1.38 mmol), $heedH_2$ (0.2 g, 1.38 mmol) and 2,2-bipyridyl (0.215 g, 1.38 mmol) were dissolved in 25 cm^3 of MeCN and stirred for 1 h. The solution was then filtered and diffused slowly with Et_2O. After 3 d black crystals of **4** were obtained in ~40% yield. Elemental analysis (%) calculated for $C_{36}H_{54}N_{10}O_{24}Cl_4Mn_4$: C 31.51, H 3.97, N 10.21. Found: C 31.43, H 4.22, N 10.36.

Synthesis of $[Mn_4O_2(heed)_2(bpy)_2Br_4]$ (5)

Anhydrous $MnBr_2$ (0.30 g, 1.38 mmol), $heedH_2$ (0.20 g, 1.38 mmol) and 2,2-bipyridyl (0.215 g, 1.38 mmol) were dissolved in MeOH (25 cm^3) and stirred for 1 h. X-Ray quality crystals of **5** were obtained in good yield (~40%) after slow evaporation of the mother liquor. Elemental analysis (%) calculated for $C_{32}H_{44}N_8O_6Br_4Mn_4$: C 32.68, H 3.77, N 9.53. Found: C 33.01, H 3.91, N 9.87.

$[\{Mn^{II}_2Mn^{IV}_2O_2(heed)_2(H_2O)_2(MeOH)_2(dca)_2\}Br_2]_n$ (6)

Anhydrous $MnBr_2$ (0.30 g, 1.38 mmol), $heedH_2$ (0.20 g, 1.38 mmol) and Na(dca) (0.13 g, 1.38 mmol) were dissolved in MeOH (25 cm^3) and stirred for 2 h. X-Ray quality crystals of **6** were obtained upon slow evaporation of the mother liquor in 42% yield after 3 d. Elemental analysis (%) calculated for $C_{10}H_{24}N_5O_6Br_1Mn_2$: C 24.02, H 4.84, N 14.00. Found: C 24.34, H 5.10, N 14.13.

Crystallography

Diffraction data were collected at 150 K using a Bruker Smart Apex CCDC diffractometer, equipped with an Oxford Cryosystems LT device, using Mo radiation. Structures **1–6** were solved using direct methods (SIR92) and refined using full-matrix least-squares against F^2 (CRYSTALS).[24]

(1). Hydrogen atoms attached to carbon atoms were placed geometrically. All hydrogens on oxygen and nitrogen atoms were located in a difference map. Hydrogens were refined subject to geometric constraints on bond lengths and angles before finally being constrained to ride on their host atoms.

(2). Disordered solvent was dealt with using Platon SQUEEZE and amounted to 2EtOH and $1H_2O$ per formula unit (see CIF file‡).

(3). The data obtained from **3** were integrated as a twin with 2 domains. Structure solution and initial refinement were carried out using data from only domain 1. Refinement was then carried out using all data from both domains. Hydrogens attached to carbon were placed geometrically. Hydrogens on nitrogen were located in a difference map and refined subject to geometric restraints. The hydroxy hydrogen atoms were placed along H-bonding interactions as the difference map indicated they were disordered due to 2 possible H-bonding interactions. Hydrogens were placed along both interactions with an occupancy of 0.5. The occupancy was not refined. All H-atoms were constrained to ride on their host atoms.

(4) and (5). The hydrogen atoms were all located in a difference map, but those attached to carbon atoms were repositioned geometrically. The H atoms were initially refined with soft restraints on the bond lengths and angles to regularise their geometry (C–H in the range 0.93–0.98, N–H in the range 0.86–0.89, N–H to 0.86, O–H = 0.82 Å) and $U \sim$ iso $\sim$ (H) (in the range 1.2–1.5 times $U_{eq.}$ of the parent atom), after which the positions were refined with riding constraints.

(6). The structure in **6** is disordered with two Mn coordination sites (Mn^{II} ions) being part occupied by MeOH and water, refined to give a total occupancy of one for each coordinating molecule. The central nitrogen on the dca ligand is also disordered and here the occupancy of the two atomic sites has been fixed at 0.5. There is also disordered solvent, which has been dealt with using Platon SQUEEZE (see refinement details). Hydrogen atoms on the disordered groups were positioned geometrically. Other H atoms were located in a difference map, and those attached to carbon atoms were repositioned geometrically. The H atoms were initially refined with soft restraints on the bond lengths and angles to regularise their geometry (C–H in the range 0.93–0.98, N–H in the range 0.86–0.89, N–H to 0.86 O–H = 0.82 Å) and $U \sim$ iso $\sim$ (H) (in the range 1.2–1.5 times $U_{eq.}$ of the parent atom), after which the positions were refined with riding constraints.

Acknowledgements

The authors gratefully acknowledge the EPSRC and the Leverhulme Trust (UK). G.S.P. thanks the Special Account for Research Grants (SARG) of the National and Kapodistrian University of Athens for support. The work was also supported by MAGMANet (NMP3-CT-2005-515767).

Notes and references

1 (*a*) A. Caneschi, D. Gatteschi, R. Sessoli, A. L. Barre, L. C. Brunel and M. Guillot, *J. Am. Chem. Soc.*, 1991, **113**, 5873–5874; (*b*) R. Sessoli, D. Gatteschi, A. Caneshi and M. A. Novak, *Nature*, 1993, **365**, 141; (*c*) R. Sessoli, H. L. Tsai, A. R. Schake, S. Y. Wang, J. B. Folting, D. Gatteschi, G. Christou and D. N. Hendrickson, *J. Am. Chem. Soc.*, 1993, **115**, 1804.

2 (*a*) V. K. Yachandra, K. Sauer and M. P. Klein, *Chem. Rev.*, 1996, **96**, 2927; (*b*) V. K. Yachandra and K. Sauer, *Biochim. Biophys. Acta*, 2004, **1655**, 140; (*c*) B. Kok, B. Forbrush and M. McGloin, *Photochem. Photobiol.*, 1970, **11**, 457; (*d*) M. Haumann, P. Liebisch, C. Muller, M. Barra, M. Grabolle and H. Dau, *Science*, 2005, **310**, 1019; (*e*) S. Mukhopadhyay, S. K. Mandal, S. Bhaduri and W. H. Armstrong, *Chem. Rev.*, 2004, **104**, 3981.

3 (*a*) K. Ferreira, T. M. Iverson, K. Maghlaoui, J. Barber and S. Iwata, *Science*, 2004, **303**, 1831; (*b*) S. Iwata and J. Barber, *Curr. Opin. Struct. Biol.*, 2004, **14**, 447; (*c*) B. Loll, W. Saenger, J. Messinger, A. Zouni and J. Biesiadka, *Nature*, 2005, **438**, 1040.

4 J. Yano, J. Kern, K. Sauer, M. J. Latimer, Y. Pushkar, J. Biesiadka, B. Loll, W. Saenger, J. Messinger, A. Zouni and V. K. Yachandra, *Science*, 2006, **314**, 821.

5 (*a*) Examples include: J. B. Vincent, C. Christmas, J. C. Huffman, G. Christou, H.-R. Chang and D. N. Hendrickson, *J. Chem. Soc., Chem. Commun.*, 1987, 236; (*b*) R. J. Kalawiec, R. H. Crabtree, G. W. Brudvig and G. K. Schulte, *Inorg. Chem.*, 1988, **27**, 1309; (*c*) J. B. Vincent, C. Christmas, H.-R. Chang, Q. Li, P. D. W. Boyd, J. C. Huffman, D. N. Hendrickson and G. Christou, *J. Am. Chem. Soc.*, 1989, **111**, 2086; (*d*) S. Wang, M. S. Wemple, J. Yoo, K. Folting, J. C. Huffman, K. S. Hagen, D. N. Hendrickson and G. Christou, *Inorg. Chem.*, 2000, **39**, 1501; (*e*) D. J. Price, S. R. Batten, K. J. Berry, B. Moubaraki and K. S. Murray, *Polyhedron*, 2003, **22**, 165; (*f*) A. J. Tasiopoulos, W. Wernsdorfer, K. A. Abboud and G. Christou, *Inorg. Chem.*, 2005, **44**, 6324; (*g*) H. Miyasaka, K. Nakata, L. Lecren, C. Coulon, Y. Nakazawa, T. Fujisaki, K. Sugiura, M. Yamashita and R. Clérac, *J. Am. Chem. Soc.*, 2006, **128**, 3770; (*h*) L. M. Wittick, L. F. Jones, P. Jensen, B. Moubaraki, L. Spiccia, K. J. Berry and K. S. Murray, *Dalton Trans.*, 2006, 1534.

6 (*a*) Examples include: V. McKee, W. B. Sheperd and S. J. Lippard, *J. Chem. Soc., Chem. Commun.*, 1985, 158; (*b*) S. Brooker, V. McKee, W. B. Sheperd and L. K. Parnell, *J. Chem. Soc., Dalton Trans.*, 1987, 2555; (*c*) K. L. Taft, A. Caneschi, C. D. Delfs, G. C. Papeafthymiou and S. J. Lippard, *J. Am. Chem. Soc.*, 1993, **115**, 11753; (*d*) G. Aromí, S. Bhaduri, P. Artus, K. Folting and G. Christou, *Inorg. Chem.*, 2002, **41**, 805; (*e*) J.-Z. Wu, E. Sellitto, G. P. A. Yap, J. Shealts and G. C. Dismukes, *Inorg. Chem.*, 2004, **43**, 5795; (*f*) B. F. Abrahams, T. A. Hudson and R. Robson, *Chem.–Eur. J.*, 2006, **12**, 7095.

7 (*a*) Examples include: J. C. Jeffrey, P. Thornton and M. D. Ward, *Inorg. Chem.*, 1994, **33**, 3612; (*b*) D. A. Bardwell, J. C. Jeffrey and M. D. Ward, *J. Chem. Soc., Dalton Trans.*, 1995, **18**, 3071; (*c*) J. Yoo, A. Yamaguchi, M. Nakano, J. Krzystek, W. E. Streib, L.-C. Brunel, H. Ishimoto, G. Christou and D. N. Hendrickson, *Inorg. Chem.*, 2001, **40**, 4604; (*d*) C. Desroches, G. Pilet, S. A. Borshch, S. Parola and D. Luneau, *Inorg. Chem.*, 2005, **44**, 9112.

8 (*a*) E. K. Brechin, *Chem. Commun.*, 2005, **41**, 5141 and references therein; (*b*) M. Manoli, R. D. L. Johnstone, S. Parsons, M. Murrie, M. Affronte, M. Evangelisti and E. K. Brechin, *Angew. Chem., Int. Ed.*, 2007, **46**, 4456.

9 C. Jocher, T. Pape, W. W. Seidel, P. Gamez, J. Reedjik and F. E. Hahn, *Eur. J. Inorg. Chem.*, 2005, 4914.

10 B. Song, J. Reuber, C. Ochs, F. E. Hahn, T. Lugger and C. Orvig, *Inorg. Chem.*, 2001, **40**, 1527.

11 G. Aromí, P. Gamez, C. Boldron, H. Koojiman, A. L. Spek and J. Reedijk, *Eur. J. Inorg. Chem.*, 2006, 1940–1944.

12 O. Delgado Friedrichs, M. O'Keeffe and O. M. Yaghi, *Acta Crystallogr., Sect. A: Found. Crystallogr.*, 2003, **59**, 515.

13 The topological analysis of the net was performed using the TOPOS program package http://www.topos.ssu.samara.ru.

14 V. A. Blatov, *Multipurpose crystallochemical analysis with the program package TOPOS, IUCr CompComm Newsletter*, 2006, p. 4.

15 (*a*) H. Miyasaka, K. Nakata, K. Sugiura, M. Yamashita and R. Clérac, *Angew. Chem., Int. Ed.*, 2004, **43**, 707; (*b*) G. S. Papaefstathiou, A. Escuer, F. A. Mautner, C. Raptopoulou, A. Terzis, S. P. Perlepes and R. Vicente, *Eur. J. Inorg. Chem.*, 2005, 879; (*c*) M. Mannini, D. Bonacchi, L. Zobbi, F. M. Piras, E. A. Speets, A. Caneschi, A. Cornia, A. Magnani, B. J. Ravoo, D. N. Reinhoudt, R. Sessoli and D. Gatteschi, *Nano Lett.*, 2005, **5**, 1435; (*d*) H. Miyasaka and M. Yamashita, *Dalton Trans.*, 2007, 399 and references therein.

16 S. R. Batten and K. S. Murray, *Coord. Chem. Rev.*, 2003, **246**, 103 and references therein.

17 A. V. Powell, R. Paniagua, P. Vaquiero and A. M. Chippendale, *Chem. Mater.*, 2002, **14**, 1220–1224.

18 Y. Wan, L. Zhang, L. Jin, S. Gao and S. Lu, *Inorg. Chem.*, 2003, **42**, 4985–4994.

19 S. Zang, Y. Su, Y. Li, Z. Ni and Q. Meng, *Inorg. Chem.*, 2006, **45**, 174–180.

20 K. Eda, Y. Iriki, K. Kawamura, T. Ikuki and M. Hayashi, *J. Solid State Chem.*, 2007, **180**, 3588–3593.

21 O. Delgado Friedrichs, M. O'Keeffe and O. M. Yaghi, *Acta Crystallogr., Sect. A: Found. Crystallogr.*, 2003, **59**, 22.

22 (*a*) J. J. Borras-Almenar, J. M. Clemente-Juan, E. Coronado and B. S. Tsukerblat, *J. Comput. Chem.*, 2001, **22**, 985; (*b*) J. J. Borrás-Almenar, J. M. Clemente-Juan, E. Coronado and B. S. Tsukerblat, *Inorg. Chem.*, 1999, **39**, 6081.

23 M. Evangelisti, F. Luis, L. J. de Jongh and M. Affronte, *J. Mater. Chem.*, 2006, **16**, 2534.

24 P. W. Betteridge, J. R. Carruthers, R. I. Cooper, K. Prout and D. J. Watkin, *J. Appl. Crystallogr.*, 2003, **36**, 1487.